Optics Letters

Toggling between active and passive imaging with an omni-resonant micro-cavity

Soroush Shabahang,[1,2] Ali K. Jahromi,[1] Abbas Shiri,[1] Kenneth L. Schepler,[1] and Ayman F. Abouraddy[1,*]

[1]CREOL, The College of Optics & Photonics, University of Central Florida, Orlando, Florida 32816, USA
[2]The Wellman Center for Photomedicine at Massachusetts General Hospital, Harvard Medical School, Cambridge, Massachusetts 02139, USA
*Corresponding author: raddy@creol.ucf.edu

Received 22 January 2019; revised 24 February 2019; accepted 25 February 2019; posted 25 February 2019 (Doc. ID 358211); published 19 March 2019

While passive illumination schemes often utilize a broadband spectral acceptance, the performance of active illumination with a laser is improved by narrowband spectral filtering at the sensor. We present an experimental demonstration of an optical cavity structure that is capable of toggling between two performance limits: narrowband resonant and broadband omni-resonant transmission. To achieve omni-resonance without modifying the cavity, the incident optical field is pre-conditioned by associating each wavelength with a particular incidence angle that enables a broad continuous spectrum to resonate with the cavity. This strategy can help seamlessly combine passive and active illumination in the same system.

https://doi.org/10.1364/OL.44.001532

Optical sensing is key to a plethora of applications including imaging, remote sensing, and process control. Two fundamental sensing methodologies can be delineated: *active* sensing where the user provides illumination, and *passive* sensing that exploits thermal emission or solar illumination. Each of these methodologies has its domain of applicability. Passive sensing can provide an overall image of the radiative intensity and spectral distribution of a scene but requires maximum throughput for optimized sensitivity, whereas active illumination can produce three-dimensional target localization. Indeed, focal plane arrays have recently been developed that collect passive imagery *and* active time-of-flight measurements of short-pulse laser illumination [1–5]. However, optimal operation of such a dual-mode sensor necessitates two spectral acceptance bandwidths. Broadband transmission ideally matching the sensor spectral sensitivity is required for passive-mode operation. On the other hand, the active sensing mode benefits from a narrow spectral bandwidth that reduces the background noise when collecting laser photons scattered from a target. Therefore, combining active and passive sensing with the same sensor array requires an optical filter that can rapidly switch between two distinct states: broadband transmission for passive imaging and narrow-line transmission with high out-of-band optical rejection for active imaging. Previously developed tunable or switchable filters include liquid crystal [6], acousto-optic [7], and micro-electro-mechanical-systems (MEMS)-based [8] devices. Each of these approaches suffers from challenges with respect to switching speed, achieving broadband transmission, out-of-band blocking, narrow bandwidth, and large aperture.

In this Letter, we report a demonstration of an in-line spectral filtering device that can be switched between two configurations: broadband and narrowband spectral transmission—while maintaining scene imaging. The device has at its core a planar Fabry–Perot (FP) cavity that transmits light only within a narrow spectral linewidth centered on a resonance, and is thus useful in this traditional configuration for *active* imaging. Nevertheless, such a cavity can be made to operate in an "omni-resonant" modality in which a continuous broadband spectrum is transmitted [9], rendering it useful for *passive* imaging. Without modifying the cavity itself, broadband transmission is achieved over multiple free spectral ranges (FSRs), and the resonant bandwidth is divorced from the cavity photon lifetime. Omni-resonance requires first introducing a precise correlation between each wavelength in the spectrum and its incidence angle. We realize this correlation using a diffraction grating system to produce a judicious angular-spectral dispersion that compensates for the angular dispersion of cavity resonances. A small angular rotation of the cavity enables switching between narrowband and broadband states, thus potentially accommodating active and passive imaging in the same system.

The concept of omni-resonance is illustrated in Fig. 1. When collimated broadband light is incident normally on a planar FP cavity, only light in a narrow linewidth $\delta\lambda$ centered at a free-space resonant wavelength $\lambda_m = 2nd/m$ is transmitted, which is determined from an axial phase-matching condition $nk_m d = m\pi$ (for integer m), where k_m is the axial component of the wave vector of the mth resonance order, d is the thickness of the cavity layer between the mirrors, and n is its refractive index [Fig. 1(a)]. At oblique incidence at an external angle θ with respect to the cavity normal, the resonant wavelengths $\lambda_m(\theta)$ blue shift with respect to their normal-incidence counterparts: $\lambda_m(\theta) = \lambda_m(0)\sqrt{1 - \frac{1}{n^2}\sin^2\theta} < \lambda_m(0)$. As such, each resonance in the spectral-angular (λ, θ) space traces a slanted trajectory.

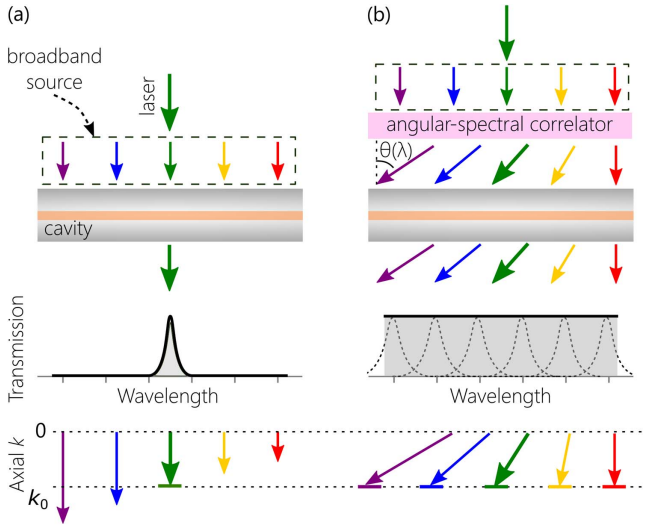

Fig. 1. Resonance versus omni-resonance in a planar optical micro-cavity. (a) A symmetric micro-cavity illuminated with broadband beam transmits light only on resonance. A monochromatic laser on resonance is also transmitted while most of the broadband light is rejected. (b) Incident light is pre-conditioned to achieve omni-resonance by introducing a wavelength-dependent incidence angle $\theta(\lambda)$, whereupon wavelengths across a continuous spectrum resonate.

The linewidth $\delta\lambda$ is inversely proportional to the cavity photon lifetime and hence also the cavity quality factor. The FSR is large in micro-cavities where d is small. Such a cavity is useful for narrowband active imaging where light is blocked except in the vicinity of the designated wavelength λ_m.

To achieve *omni*-resonance, i.e, continuous broadband resonant cavity transmission, we do not manipulate the cavity itself in any way. Instead, we pre-condition the broadband radiation to assign each wavelength λ to a particular incidence angle $\theta(\lambda)$, which is selected such that *every* wavelength satisfies the axial phase-matching condition, i.e., the axial component of the wave vector is *constant* across the whole spectrum [9]. The wavelength-dependent *external* incidence angle $\theta(\lambda)$ is given by

$$\sin[\theta(\lambda)] = \pm n\sqrt{1 - \left(\frac{\lambda}{\lambda_m(0)}\right)^2}. \quad (1)$$

The effect of this pre-conditioning is to de-slant the resonance trajectory in the spectral-angular domain, thereby rendering the cavity transmissive over a large bandwidth *independently* of the cavity linewidth. Realizing such a field configuration requires a dispersive element (e.g., a diffraction grating) to spread the spectrum $\Delta\lambda$ over an angular extent $\Delta\theta$ that depends on the FP cavity parameters n and d, and the resonance order m. Note, however, that normal incidence on a grating that is parallel to the cavity produces the opposite-signed angular dispersion. The sign of the angular dispersion can be switched by introducing a relative angular tilt between the cavity and the grating [9]. This tilt introduces a geometric transformation capable of switching the sign of the angular dispersion, as is realized in certain butterfly wing-scales [10,11]. Alternatively, nanophotonic systems can achieve a similar effect [12,13]. We proceed to describe the realization of an omni-resonant system that can be switched to the traditional narrowband resonant condition or block light altogether.

The experimental arrangement to realize omni-resonance is depicted schematically in Fig. 2. With the help of a beam splitter, a collimated incoherent broadband beam from a 100-W white light lamp is combined with a monochromatic laser at a wavelength of ∼532 nm. The combined fields are directed to the omni-resonant cavity after first transmitting through an object in the form of a transparency displaying a Pegasus, which is removed when we characterize the omni-resonant cavity itself. The field (both white light and the laser beam) is passed through two 5-mm-diameter irises followed by a $2 \times 1\text{-mm}^2$ rectangular aperture to improve the collimation.

At the heart of the system is a symmetric FP resonator consisting of two Bragg mirrors sandwiching a ≈4-μm-thick silica layer. Each Bragg mirror consists of four bilayers of TiO_2 and SiO_2 (thicknesses 60 nm and 94 nm and refractive indices 2.38 and 1.46, respectively, on a 1-mm-thick BK7 substrate) to produce a spectral reflection band in the range of 500–600 nm (which sets the maximum achievable omni-resonant bandwidth in our experiment), a linewidth $\delta\lambda \approx 0.8$ nm at a resonance wavelength $\lambda_o \approx 533.2$ nm, and a FSR of ∼23 nm; see Fig. 3(a) for the measured transmission spectrum of the bare cavity. With these parameters, the required angular dispersion to achieve omni-resonance is $\beta = \frac{\Delta\theta}{\Delta\lambda} = 0.35°/\text{nm}$.

Prior to the FP resonator, the field is incident on a diffraction grating (1800 lines/mm; Thorlabs GR25-1850) at an angle of 50° with respect to the grating normal. The first diffraction order from this grating provides an angular-spectral dispersion of $\beta \approx 0.09°/\text{nm}$. We increase β to the required value using a lens with focal length $f = 25$ mm [9] that "amplifies" the angular spread. The field then impinges on the FP resonator tilted an angle φ from its orientation normal to the central wavelength of 532 nm (Fig. 2, inset). The measured transmitted spectrum with φ is plotted in Fig. 3(b) where the de-slanting of the resonances in the spectral-angular domain is clear. At several values φ_m of the tilt angle (e.g., $\varphi_m \approx 30°$, 40°, and 50°) *achromatic* resonances appear in the spectrum, indicating that a continuous wavelength range resonates simultaneously over a bandwidth of ∼50 nm extending over multiple FSRs. Note that each achromatic resonance at φ_m

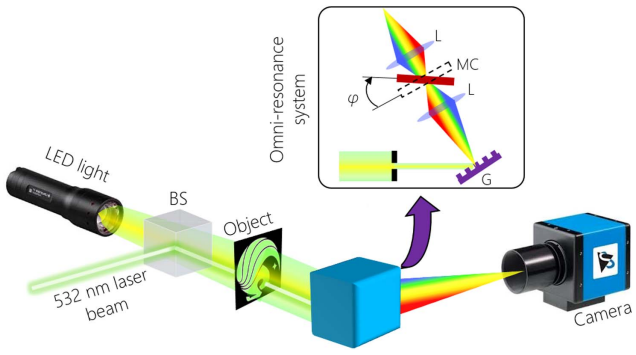

Fig. 2. Experimental setup for toggling between active/resonant and passive/omni-resonant imaging modalities. The omni-resonant arrangement consists of a micro-cavity (MC), a diffraction grating (G), and a lens (L). After the combined action of the grating and lens, the field is endowed with the requisite spectral-angular dispersion distribution to resonate within the micro-cavity over a continuous broadband spectrum. The laser wavelength is chosen to lie along the optical axis of the system. To distinguish between broadband light and the laser spot, the laser beam is directed to transmit at the "eye" of the Pegasus object.

corresponds to a single resonance of the bare cavity that has been completely de-slanted, rendering the cavity omni-resonant [9]. Four configurations associated with different tilt angle settings can be delineated [Fig. 3(c)]: transmission of the laser light only while blocking the out-of-band white light (e.g., $\varphi \approx 34°$), which corresponds to narrowband operation; blocking of all light (e.g., $\varphi \approx 36°$); transmitting broadband light and partially suppressing the laser light (e.g., $\varphi \approx 50°$); and transmitting all light (e.g., $\varphi \approx 52°$), or broadband operation.

It may appear at this point that the field has been "scrambled" through the impact of the diffraction grating, such that the omni-resonant system cannot image an object through the grating. To dispel this notion, we now carry out the experiment with a 1×1 cm^2 transparency depicting a "Pegasus" in the path of the input field before passing through the omni-resonant cavity. The white-light beam covers the entire object, while the laser is incident only on the "eye" of the Pegasus. We place a second lens with $f = 25$ mm after the FP resonator to direct the transmitted light to a color CCD camera (The ImagingSource, DFK 33UX178). The distance from the cavity to the second lens is adjusted to form an image of a given input plane (preceding the grating) to the CCD plane. Although the grating and lens spread the spectrum, the second lens recombines the spectrum and produces an image at the CCD of an object plane preceding the grating. If subsequent optical processing of the field is desired, a second grating can be placed at the CCD plane.

The four spectral configurations delineated above can now be examined in an imaging configuration, as shown in Fig. 4: (1) in Fig. 4(a) at $\phi = 36°$, the entire spectrum is blocked. (2) In Fig. 4(b) at $\phi = 34°$, only the laser light (appearing at the Pegasus eye) is transmitted, corresponding to the narrowband transmission configuration. The weak broadband transmission of the Pegasus image is suppressed relative to the laser beam peak intensity by a rejection ratio of at least 11 dB (the camera pixels at the laser light location were saturated, so the rejection ratio in fact exceeds this value). (3) In Fig. 4(c) at $\phi = 50°$, the white-light beam is transmitted while the laser light is partially suppressed. (4) In Fig. 4(d) at $\phi = 52°$, both the white-light beam and the laser beam are transmitted across the omni-resonant bandwidth, corresponding to the broadband transmission configuration. All of these detailed characteristics are in excellent agreement with calculations of the transmission of our omni-resonant device. The imaging resolution of our system is attested to by the transmittance of the details of the Pegasus object. A further functionality that may be envisioned is the suppression of a particular wavelength while maintaining

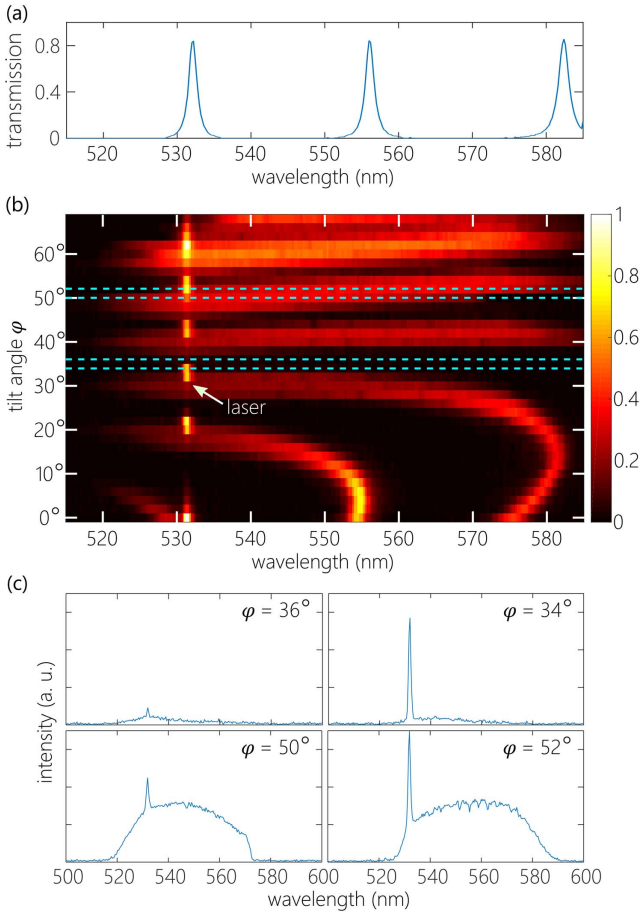

Fig. 3. (a) Spectral transmission through the cavity when illuminated by a normally incident broadband beam. (b) Spectral transmission measurements through the cavity as a function of the cavity tilt angle φ for the angularly dispersed beam in Fig. 2. We highlight the tilt angles that are used with dashed lines and the wavelength of the laser. (c) Panels are measured light intensity transmitted versus wavelength at selected cavity angles of $\varphi = 34°$, 36°, 50°, and 52°.

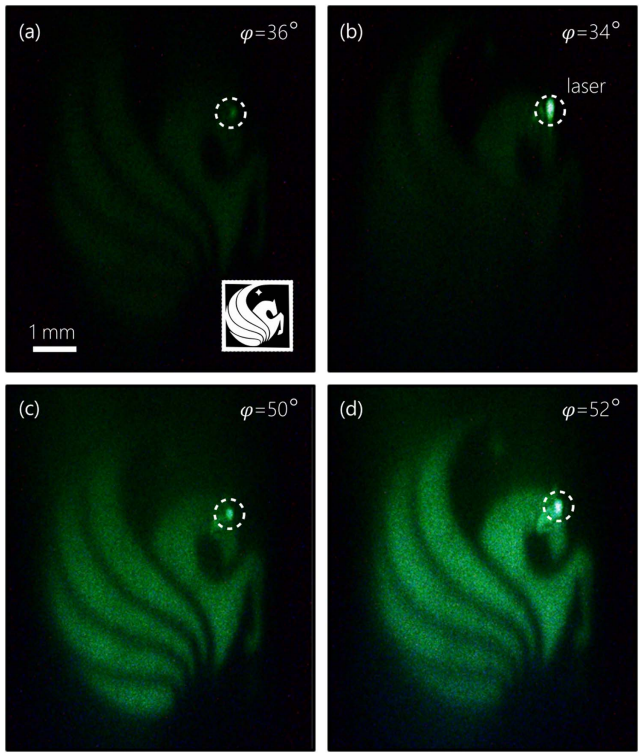

Fig. 4. Singly resonant and omni-resonant imaging modalities. Panels are images captured by the CCD camera at specific cavity tilt angles (φ). (a) Spectral rejection: $\varphi = 36°$, where the entire spectrum is blocked; inset is original Pegasus object. (b) Resonant imaging: $\varphi = 34°$, corresponding to resonant imaging where only the laser beam is transmitted. (c) Partial omni-resonant condition: $\varphi = 50°$, where broadband light is transmitted and the laser wavelength is not fully transmitted. (d) Omni-resonant imaging: at $\varphi = 52°$ both the broadband and laser light are transmitted.

omni-resonance. This can be achieved by adding a narrowband rejection filter to the cavity or inserted into the optical path.

Further investigations beyond this proof-of-principle demonstration can be directed along several avenues. First, the toggling between the resonant and omni-resonant imaging conditions through a rotation of the cavity can be achieved instead via temperature control or piezo-electric displacement of the cavity to change d, current injection to modify the index [14], MEMS-based cavity mirrors [8], or deformable (e.g., liquid) lenses, which can help improve the system's speed and stability. Second, metasurfaces [15] may provide the necessary angular-spectral dispersion for omni-resonance and thus replace the diffraction grating and lens with a thin flat surface component. Third, it is important to determine what is the limit on achievable omni-resonant bandwidth, e.g., can omni-resonance be achieved over the full visible spectrum? Fourth, omni-resonance can be implemented in any spectral window of interest, by first constructing a cavity operating in that spectral window (whether in the ultraviolet or the infrared, e.g.), and then selecting the appropriate diffraction grating. Finally, we have exploited the resonant nature of the cavity for spectral filtering, but other resonant effects may be harnessed, e.g., resonant optical delays, field-enhanced nonlinearities [16], and coherent perfect absorption [17–20].

It is worth comparing our strategy for achieving omni-resonance with previous attempts at constructing a so-called white-light cavity [21] by inserting atomic [22,23] or nonlinear [24] media into the cavity. Only narrow spectral broadening (multiple resonance linewidths at best) has been observed using these approaches compared to the multiple FSRs achieved using our strategy. Moreover, it is now understood that placing linear optical elements within the cavity (e.g., diffraction gratings [25] or chirped mirrors [26]) cannot achieve this effect. Micro-resonators with broad continuous resonant spectra have been produced [27,28], but they are not useful for imaging applications. Our methodology does not modify the cavity itself in any way, and instead only pre-conditions the incident radiation spatio-spectral distribution.

Finally, we note that our strategy is a variant on the concept of "space–time" wave packets [29–32], which are pulsed beams that undergo rigid transport in free space without diffraction or dispersion. Omni-resonance and space–time wave packets both require introducing tight spatio–temporal spectral correlations into the field by associating each wavelength with a particular angle of incidence or spatial frequency. The distinction is in the prescribed dispersion relation: omni-resonance requires matching the intrinsic spatio–temporal dispersion of a resonator, whereas space–time wave packets require nulling the space–time coupling associated with diffraction. Both approaches—omni-resonant cavities and space–time wave packets—thus extend the concept of "classical entanglement" from discrete modes [33] to continuous degrees of freedom of the field [34].

In conclusion, we have demonstrated an experimental scheme for incorporating two distinct functionalities in the same optical system: narrowband resonant filtering and broadband omni-resonance. Both functionalities are realized in-line in an imaging configuration.

Funding. Air Force Office of Scientific Research (AFOSR) (FA9550-14-1-0037); Office of Naval Research (ONR) (N00014-17-1-2458).

Acknowledgment. We thank M. L. Villinger for helpful discussions.

REFERENCES

1. M. A. Albota, R. M. Heinrichs, D. G. Kocher, D. G. Fouche, B. E. Player, M. E. O'Brien, B. F. Aull, J. J. Zayhowski, J. Mooney, B. C. Willard, and R. R. Carlson, Appl. Opt. **41**, 7671 (2002).
2. R. M. Brubaker, M. H. Ettenberg, M. T. O'Grady, M. A. Blessinger, and J. C. Dries, Proc. SPIE **5406**, 10 (2004).
3. M. E. DeFlumere, "Dual-mode focal plane array for missile seekers," U.S. patent 6,864,965 B2 (March 8, 2005).
4. M. S. Oh, H. J. Kong, T. H. Kim, S. E. Jo, B. W. Kim, and D. J. Park, J. Opt. Soc. Am. A **28**, 759 (2011).
5. M. A. Itzler, E. M. Owens, K. Patel, X. Jiang, K. Slomkowski, and S. Rangwala, in *Imaging and Applied Optics*, OSA Technical Digest (CD) (Optical Society of America, 2011), p. LThA3.
6. J. Y. Hardeberg, F. Schmitt, and H. Brettel, Opt. Eng. **41**, 2532 (2002).
7. N. Gupta, R. Dahmani, M. S. Gottlieb, L. J. Denes, B. Kaminsky, and P. Metes, Proc. SPIE **3718**, 10 (1999).
8. J. S. Milne, J. M. Dell, A. J. Keating, and L. Faraone, J. Microelectromech. Syst. **18**, 905 (2009).
9. S. Shabahang, H. E. Kondakci, M. L. Villinger, J. D. Perlstein, A. El Halawany, and A. F. Abouraddy, Sci. Rep. **7**, 10336 (2017).
10. J. P. Vigneron, P. Simonis, A. Aiello, A. Bay, D. M. Windsor, J.-F. Colomer, and M. Rassart, Phys. Rev. E **82**, 021903 (2010).
11. G. England, M. Kolle, P. Kim, M. Khan, P. Muñoz, E. Mazur, and J. Aizenberg, Proc. Natl. Acad. Sci. USA **111**, 15630 (2014).
12. A. A. High, R. C. Devlin, A. Dibos, M. Polking, D. S. Wild, J. Perczel, N. P. Leon, M. D. Lukin, and H. Park, Nature **522**, 192 (2015).
13. E. Arbabi, A. Arbabi, S. M. Kamali, Y. Horie, and A. Faraon, Optica **4**, 625 (2017).
14. L. S. Yu, Q. Z. Liu, Z. F. Guan, and S. S. Lau, Appl. Phys. Lett. **68**, 1546 (1996).
15. N. Yu and F. Capasso, Nat. Mater. **13**, 139 (2014).
16. E. Makri, H. Ramezani, T. Kottos, and I. Vitebskiy, Phys. Rev. A **89**, 031802(R) (2014).
17. Y. D. Chong, L. Ge, H. Cao, and A. D. Stone, Phys. Rev. Lett. **105**, 053901 (2010).
18. W. Wan, Y. Chong, L. Ge, H. Noh, A. D. Stone, and H. Cao, Science **331**, 889 (2011).
19. M. L. Villinger, M. Bayat, L. N. Pye, and A. F. Abouraddy, Opt. Lett. **40**, 5550 (2015).
20. L. N. Pye, M. L. Villinger, S. Shabahang, W. D. Larson, L. Martin, and A. F. Abouraddy, Opt. Lett. **42**, 151 (2017).
21. A. Wicht, K. Danzmann, M. Fleischhauer, M. Scully, G. Müller, and R. H. Rinkleff, Opt. Commun. **134**, 431 (1997).
22. G. S. Pati, M. Salit, K. Salit, and M. S. Shahriar, Phys. Rev. Lett. **99**, 133601 (2007).
23. H. Wu and M. Xiao, Phys. Rev. A **77**, 031801(R) (2008).
24. H. N. Yum, J. Sheuer, M. Salit, P. R. Hemmer, and M. S. Shahriar, J. Light. Technol. **31**, 3865 (2013).
25. S. Wise, V. Quetschke, A. J. Deshpande, G. Mueller, D. H. Reitze, D. B. Tanner, B. F. Whiting, Y. Chen, A. Tünnermann, E. Kley, and T. Clausnitzer, Phys. Rev. Lett. **95**, 013901 (2005).
26. H. N. Yum, X. Liu, P. R. Hemmer, J. Scheuer, and M. S. Shahriar, Opt. Commun. **305**, 260 (2013).
27. A. A. Savchenkov, A. B. Matsko, and L. Maleki, Opt. Lett. **31**, 92 (2006).
28. D. V. Strekalov, A. A. Savchenkov, E. A. Savchenkova, and A. B. Matsko, Opt. Lett. **40**, 3782 (2015).
29. H. E. Kondakci and A. F. Abouraddy, Nat. Photonics **11**, 733 (2017).
30. H. E. Kondakci and A. F. Abouraddy, Phys. Rev. Lett. **120**, 163901 (2018).
31. H. E. Kondakci and A. F. Abouraddy, arXiv:1810.08893 (2018).
32. B. Bhaduri, M. Yessenov, and A. F. Abouraddy, Optica **6**, 139 (2019).
33. K. H. Kagalwala, G. Di Giuseppe, A. F. Abouraddy, and B. E. A. Saleh, Nat. Photon. **7**, 72 (2013).
34. H. E. Kondakci, M. A. Alonso, and A. F. Abouraddy, arXiv:1812.10566 (2018).